High External Quantum Efficiency Green Light Emitting Diodes on Stress-Manipulated AlNO Buffer Layers

Aimin Wang, Kaixuan Chen, Jinchai Li, and Junyong Kang

***Abstract*—We demonstrated high-brightness InGaN/GaN green light emitting diodes (LEDs) with ex-situ sputtered stress-manipulated AlNO buffer on 4-inch patterned sapphire substrates. The lattice constant of the AlNO buffer was adjusted by oxygen flow. As a result, the dislocation density and the in-plane compressive stress caused by lattice mismatch were greatly reduced, while the interface quality of the InGaN/GaN multiple quantum wells and the uniformity of the indium composition were greatly improved. At 20A/cm^2, the external quantum efficiency and wall plug efficiency of the 526.4-nm-green LEDs grown on the sputtered AlNO buffer reached 46.1% and 41.9%, which were both higher than reported values.**

***Index Terms*—AlNO buffer, pattern sapphire substrate, InGaN/GaN quantum well, light-emitting diode, green gap.**

I. Introduction

LIGHT emitting diodes (LEDs) have been widely used in general lighting, backlight unit, display, agriculture and communications. The development of solid-state lighting based on LEDs offers an opportunity to significantly reduce worldwide energy consumption [1]–[3]. Nevertheless, the LED efficiencies with different colors are unbalanced: the efficiency of the LEDs in the green wavelength region is much lower than that of the blue and red. This problem is known as the "green gap". On one hand, for the LEDs made from $(Al_xGa_{1-x})_{0.5}In_{0.5}P$, their external quantum efficiency (EQE) is very high in the red region. However, the energy band of $(Al_xGa_{1-x})_{0.5}In_{0.5}P$ will change from direct band gap to indirect band gap when the Al composition x is higher than 0.5, corresponding to the emission of green-yellow wavelength around 570 nm. The direct-indirect transition in the band gap of $(Al_xGa_{1-x})_{0.5}In_{0.5}P$ leads to a sharp decrease in the EQE [4], [5]. On the other hand, although InGaN-based LEDs grown on pattern sapphire substrate (PSS) have achieved great success in blue region, it is still challenging to obtain high EQE green LEDs with high indium composition [3]. The large lattice mismatch and thermal expansion coefficient difference between the epi-layer and the substrate give rise to a high density of threading dislocations and a large residual strain in the LED structures [6]–[8]. Furthermore, the contrasting thermodynamic and structural properties of InN and GaN lead to low miscibility, making it difficult to grow high-quality green-emitting InGaN/GaN multiple quantum wells (MQWs) [9]. Several methods have been used to improve the EQE of green LEDs, such as the use of pattern sapphire substrates, non-polar or semi-polar substrates [10], AlGaN ternary quantum well protective layers [11], [12], sandwich MQW growth process [13], [14], and controlling the strain, field, electronic band mechanism to reduce the influence of QCSE [15], [16] The EQE of the green LEDs has been improved to reach 40%. In spite of this, it is still much lower than that of blue LEDs [17].

In this paper, the mismatch between the nitride epi-layers and the substrate was manipulated with ex-situ sputtered AlNO buffer on 4-inch PSS. The lattice constants of the AlNO buffer layers and the dislocation densities of full LED structures were investigated by X-ray diffraction and rocking curve analysis. The influence of the buffer layers on the InGaN quantum wells was examined by analyzing the reciprocal space mappings of epi-layers. Finally, both the enhancements of photoluminescence (PL) and electroluminescence were confirmed to significantly bridge the green gap in the wall plug efficiency as well as the external quantum efficiency.

II. Experiment

A 45-nm thick AlNO buffer layer was deposited on a 4-inch c-plane PSS using physical vapor deposition (PVD) at 700 °C. The oxygen content in the AlNO buffer layer was adjusted during sputtering by using different O_2 flow rates of 0, 1, 2, 3, and 4 sccm (labeled as Buffer A, B, C, D, and E, respectively). Thereafter, InGaN-based green LEDs were grown on the buffer layer using metal organic vapor phase epitaxy (MOVPE). The growth precursors were trimethylgallium (TMGa), triethylgallium (TEGa), trimethylindium (TMIn), ammonia (NH_3), silane (SiH_4), and bis-cyclopentadienyl magnesium (Cp_2Mg). The LED structures

Manuscript received October 26, 2021; revised December 23, 2021; accepted January 1, 2022. Date of publication January 6, 2022; date of current version June 15, 2022. This work was supported by the Key Scientific and Technological Program of Xiamen, China, under Grant 3502Z20191016. *(Corresponding authors: Kaixuan Chen; Junyong Kang.)*

Aimin Wang, Jinchai Li, and Junyong Kang are with the Engineering Research Centre of Micro-Nano Optoelectronic Materials and Devices, Ministry of Education, Fujian Key Laboratory of Semiconductor Materials and Applications, CI Centre for OSED, Department of Physics, Xiamen University, Xiamen 361005, China (e-mail: wam07@foxmail.com; jinchaili@xmu.edu.cn; jykang@xmu.edu.cn).

Kaixuan Chen is with the Xiamen Changelight Company, Ltd., Xiamen, Fujian Province 361101, China (e-mail: ckx@changelight.com.cn).

Digital Object Identifier 10.1109/JPHOT.2022.3140775

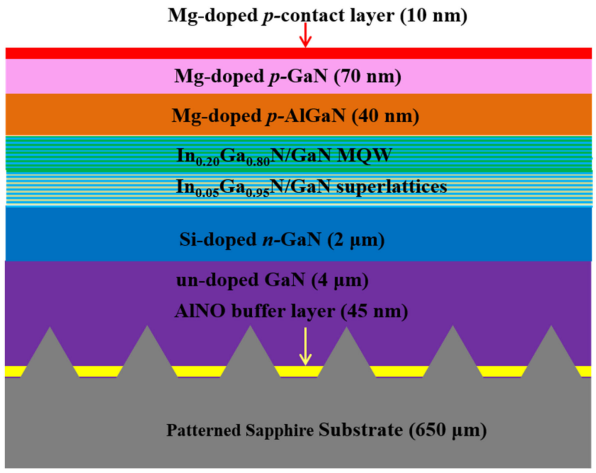

Fig. 1. Cross-sectional schematics of full LED structure with an AlNO buffer layer.

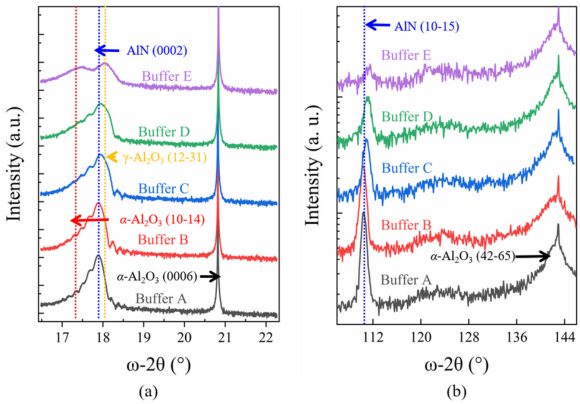

Fig. 2. X-ray diffraction ω-2θ scan along (a) (0002) and (b) (10-15) planes.

comprised a 4-μm-thick undoped GaN layer, a 2-μm-thick Si-doped n-GaN layer, 9 pairs of $In_{0.05}Ga_{0.95}N$/GaN superlattices, 10 pairs of $In_{0.20}GaN_{0.80}$/GaN MQWs, 40-nm-thick p-type AlGaN electron-blocking layer (EBL), 70-nm-thick p-GaN, and 10-nm-thick heavily Mg doped $p+$-GaN as the contact layer. The LED epitaxial wafers on different buffer layers were named as LED A, B, C, D, and E. The green LED device structure was illustrated in the cross-sectional schematic shown in Fig. 1.

The material quality of the AlNO buffer layers and epi-layers were characterized using high-resolution X-ray diffraction (XRD) (Philips X'Pert MRD). The optical properties of full LED structures were analyzed using an epitaxial photoluminescence spectrum scanning imager (Chn-Top Optical-Electronic IM-3000). The performance of the LEDs was measured using a high accuracy array spectro-radiometer (Everfine HAAS-2000).

III. Results and Discussions

A. AlNO Buffer Layers

The quality of the AlNO buffer layers was analyzed by using XRD. The ω-2θ scanning curves of Buffer A, B, C, D, and E on (0002) plane were shown in Fig. 2(a). It showed that in the absence of oxygen (Buffer A), the ω-2θ curve had only one diffraction peak (blue dotted line) of the (0002) plane of AlN [18] and one diffraction peak (black dotted line) of the (0006) plane of the substrate (α-Al2O3) [19]. Moreover, the AlN thin films prepared using the PVD sputtering without oxygen incorporation had a hexagonal wurtzite structure. A small peak of the γ-Al2O3 (12-31) plane was observed (yellow dotted line) when the O_2 flow rate was 1 sccm (Buffer B) [20]. With an increasing O_2 flow rate, the diffraction peaks of AlN (0002) gradually merged with the small peak of γ-Al_2O_3 (12-31) plane, indicating the infusion of oxygen in the AlN structure of the hexagonal system. Oxygen atoms partly substitute nitrogen atoms to form an AlNO ternary buffer layer while the AlNO layer still kept the hexagonal wurtzite structure. When the O_2 flow rate exceeded 4 sccm (Buffer E), the crystal structure of AlN was seriously changed because of the higher chemical activity of oxygen. This caused obvious phase separation in the buffer and resulted in double peaks in the diffraction curve of Buffer E. With the destruction of the wurtzite structure, Buffer E became unsuitable for the subsequent epitaxial growth.

TABLE I
Lattice Constants of AlNO Buffer Layers and Lattice Mismatch With α-Al_2O_3

Buffer	O_2 flow rate (sccm)	Lattice constant (nm)	a-axis mismatch with α-Al_2O_3 (%)
A	0	c = 0.4988 a = 0.3111	-13.4
B	1	c = 0.4988 a = 0.3081	-12.2
C	2	c = 0.4988 a = 0.3031	-10.4
D	3	c = 0.4988 a = 0.2971	-8.3
E	4	c = 0.4988 a = 0.2941	-7.2

The ω-2θ scanning curves of Buffer A, B, C, D, and E on (10-15) plane were shown in Fig. 2(b). When the O_2 flow rate was 0 (Buffer A), the diffraction peak (blue dotted line) of the AlNO (10-15) plane had a large angle difference with the diffraction peak (black dotted line) of the α-Al_2O_3 (42-65) plane. With an increasing O_2 flow rate, the diffraction peak of the AlNO (10-15) plane gradually moved closer to the peak of the α-Al_2O_3 (42-65) plane, indicating that the mismatch of a-axis between the buffer layer and the PSS was reduced. The lattice constants of AlNO buffer layers calculated from XRD were listed in Table I. The in-plane lattice constant a and the lattice mismatch with α-Al_2O_3 decreased with increasing oxygen content. The calculated lattice mismatch for Buffer A was -13.4%, which was consistent with the reported data [10]. Although the lattice mismatch for Buffer E reached the lowest value among all of the buffers, its wurtzite structure was destroyed, indicated by its weak diffraction peak in Fig. 2(b). Therefore, it was not suitable to be used as a buffer layer for subsequent epitaxial growth. Buffer D with an O_2 flow rate of 3 sccm was more suitable for subsequent epitaxial growth.

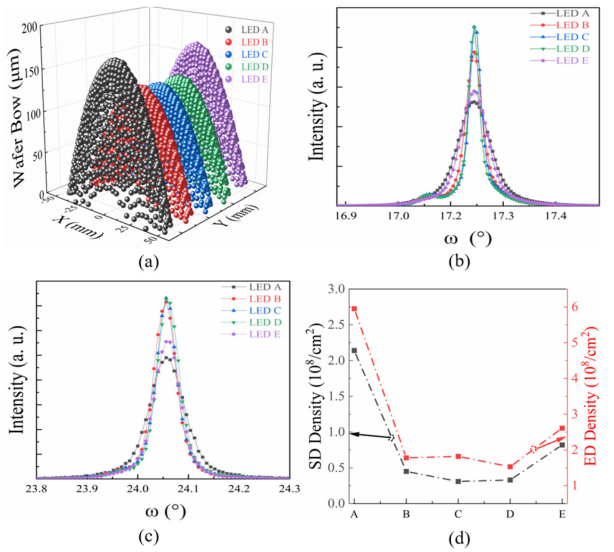

Fig. 3. (a) Wafer bow distribution in space. (b) Rocking curves of (0002) plane of different LEDs. (c) Rocking curves of ~~the~~ (10-12) plane of different LEDs. (d) Corresponding screw and edge dislocation densities of different LEDs.

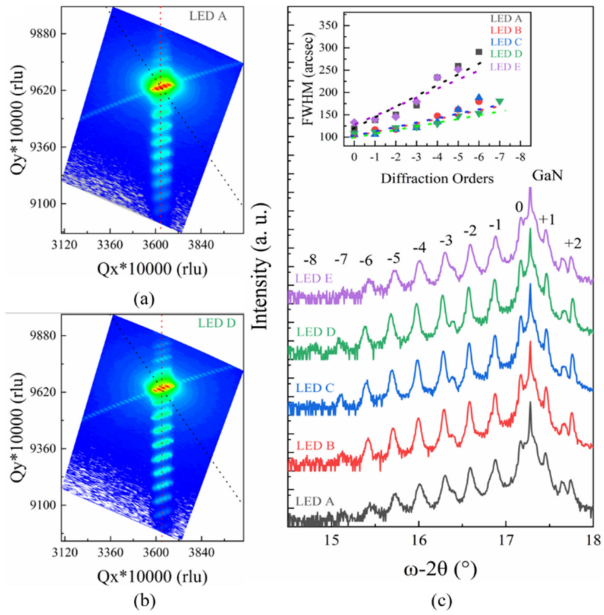

Fig. 4. (a)–(b) Reciprocal space mappings (RSM) of LED A and LED D on (10-15) plane. Vertical (red dot) and inclined (black dot) lines represent positions of a fully strained and fully relaxed layer grown on GaN, respectively. (c) ω-2θ curves of (0002) plane of different LEDs. Inset shows FWHM of diffraction peaks with different diffraction orders.

B. Full LED Structures

Following the growth and characterization of the AlNO buffer layers with different O_2 flow rates (Buffer A-E), green LEDs (named as LED A-E) with the same structure and an emission wavelength of 525 nm were grown on top of these AlNO buffer layers. As mentioned above, the oxygen content in the AlNO film could effectively reduce the lattice mismatch between AlNO and PSS. Therefore, the in-plane biaxial stress caused by the lattice mismatch should also be reduced. For LED A-E, the wafer bow mapping of each LED was obtained at room temperature (293 K), as shown in Fig. 3(a). For the full LED structure grown on the pure AlN buffer layer (LED A), it had the largest in-plane compressive stress because of the biggest lattice mismatch between its AlNO buffer and PSS. In LED B, C, and D, the stress and the wafer bow values were significantly reduced due to the decrescent lattice mismatch between their AlNO buffer layers and PSS. Although the lattice mismatch for LED E was the smallest among all LEDs, the ω-2θ scan curves along the (0002) and (10-15) planes showed that its buffer layer had obvious phase separation, which might affect subsequent epitaxial growth and resulted in a higher in-plane stress. The trend of the in-plane stress in the full LED structure was consistent with that of the lattice mismatch between the AlNO buffer and PSS.

In order to determine the effect of different buffer layers on the epi-layer quality of the full LED structure, the rocking curves of the (0002) and (10-12) planes of different LEDs were measured using high-resolution XRD, and the dislocation density of different LEDs was estimated. As shown in Fig. 3(b) and (c), the full width at half maximum (FWHM) of the (0002) and (10-12) XRD rocking curves decreased with increasing O_2 flow rates in the buffer layers (LED A -D), which indicated that the crystal qualities of the epi-layers were improved. By further increasing the O_2 flow rate in the buffer layer of LED E, the FWHM of the rocking curves was broaden because its buffer layer quality was deteriorated. The decrescent lattice mismatch of the buffer layer significantly improved the crystal quality of the epi-layer and reduced the density of screw dislocations (SD) and edge dislocations (ED). The SD and ED densities of LED A-E can be calculated by using the following formula [21], [22]:

$$D=\frac{\beta_\alpha^2}{2\pi b^2 \ln 2} \tag{1}$$

where β_α is the diffraction FWHM of the (0002) or (10-12) rocking curves, and $\boldsymbol{b}$ is the Burgers vector of the dislocation. The growth conditions of different buffer layers significantly and directly influence the dislocation density of the final epi-layers. The SD and ED densities of different LEDs were calculated using (1) and the results were presented in Fig. 3(d). With different oxygen content in the buffer layers, the lattice mismatch between the buffer layer and the PSS was effectively reduced, thus the dislocation density of the epi-layer also decreased.

In order to examine the influence of different buffer layers on the LED performance, the relaxation between the InGaN quantum wells and the GaN barriers in the MQW layer of different LEDs was measured. The reciprocal space mappings (RSM) of LED A and LED D on the (10-15) plane were shown in Fig. 4(a) and (b). According to the RSM, the InGaN well layers had exactly the same a-axis lattice constant as the GaN barriers in all LEDs, which indicated that the InGaN well layers were fully strained. The difference in the resolution of higher-order diffraction spots indicated that the MQW qualities of individual LEDs were quite different. For LED A and LED E, the edges of their diffraction spots were blur, and the -7th order diffraction spot was hardly recognized. It meant the inferior quality or a larger composition fluctuation in the MQWs. For LED B, C, and D, the edges of the diffraction spots were sharp and the -8th order diffraction spot was clearly recognized, which

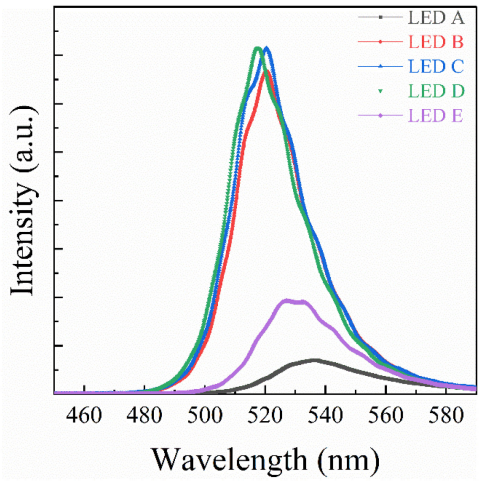

Fig. 5. Photoluminescence spectra of different LEDs.

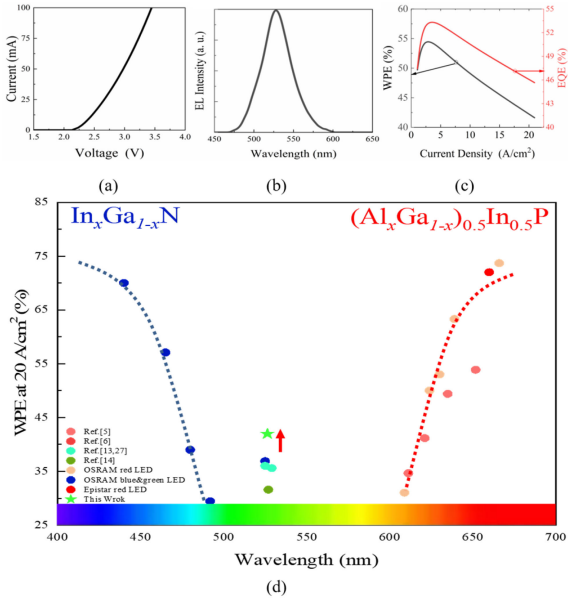

Fig. 6. (a) Dependence of voltage on current density, inset shows electroluminescence (EL) spectrum at 20 A/cm^2. (b) Dependence of WPE and EQE on current density. (c) WPE of nitride and phosphide LEDs as a function of emission wavelength at 20 A/cm^2 [5], [6], [13], [14], [27].

demonstrated a much better quality of the MQWs. To further examine the differences in MQW quality among different LEDs, the (0002) plane ω-2θ scan of all LEDs were measured. As shown in Fig. 4(c), the InGaN diffraction peaks of different LEDs had the same period, which indicated that all the LEDs had exactly the same MQW structure and indium composition in the InGaN wells. The superlattice period thickness (157 Å $\pm$ 2 Å for all LEDs) and indium composition (20 $\pm$ 0.1% for all LEDs) obtained from fitting were confirmed by direct calculation using the program Philips X'Pert Epitaxy 4.0 [23], [24]. At the same time, there were obvious differences in the FWHM of individual diffraction peaks for all LEDs, as shown in the inset of Fig. 4(c). For the 0th InGaN diffraction peaks, LED B, C, and D had much smaller FWHM than LED A and LED E. It testified that LED B, C, and D had much better MQW qualities, because the decreasing in-plane stress reduced the lattice defects in the MQWs. Furthermore, although the FWHM of the diffraction peaks of all LEDs increased with the diffraction order, the increasing rates of LED B, C, and D were much smaller than that of LED A and LED E. It was known that for the MQW structures the FWHM of satellite peaks of ω-2θ scan curves will be broadened with increase of the satellite peak's order by the rough interfaces between wells and barriers [25]–[27]. As shown in the inset of Fig. 4(c), the slopes of the fitting curves represented the roughness of the MQW interface. The interface roughness obtained according to the slope values were about 1.55%, 0.63%, 0.60%, 0.46%, and 1.22% for LED A, B, C, D, and E, respectively. This result indicated that LED B, C, and D had better periodic consistency, indium component uniformity, and interface smoothness than LED A and LED E. Among all the LEDs, LED D had the sharpest MQW interface and the smallest composition fluctuation due to the smallest in-plane stress.

The optical properties of different LEDs were characterized by photoluminescence. The PL integrated intensity (INT) ratios of different LEDs were 1.0: 7.0: 7.4: 7.5: 2.7, according to Fig. 5. Notably, the PL INTs of LED B, C, and D were much higher than LED A and LED E. The PL peak wavelengths of LED A-E were 535.6 nm, 520.6 nm, 520.4 nm, 517.5 nm and 527.3 nm, respectively. There was a large blue shift for LED B, C, and D. The polarization field caused bandgap bending, emission spectrum red shift, and radiative recombination reduction in MQWs, which was known as QCSE [8]. The enhanced INT and the shorter wavelength indicated that the QCSE in LED B, C, and D had been greatly alleviated. Based on this result, it was concluded that AlNO buffer layers could effectively reduce the in-plane stress due to the lattice mismatch between PSS and LEDs, thus alleviate the QCSE caused by piezoelectric polarization field and increase radiative recombination. As a result, LED D with the smallest mismatch had the highest PL INT.

A 0.28$\times$0.35 mm^2 green LED chip with an emission wavelength of 526.4 nm was fabricated based on LED D. Dependence of voltage on current density and EL spectrum were shown in Fig. 6(a), and the dependence of WPE and EQE on current density was shown in Fig. 6(b). WPE is defined as the ratio of emitted optical power to injected electrical power ($WPE = \frac{P}{IV}$), where P is the optical power, I is the current and V is the forward voltage. And EQE is defined as the ratio of the number of photons emitted from the LED to the number of electrons passing through the device ($EQE = \frac{P/(h\nu)}{I/e} = \frac{P\lambda}{I} * \frac{e}{Ch}$), where ν is the emission light frequency of LEDs, λ is the emission wavelength of LEDs, e is the elementary charge, C is the velocity of light, h is the Planck constant.

At a typical working current density of 20 A/cm^2, the chip exhibited a low forward voltage of 2.59 V and a high optical power of 21.6 mW. Furthermore, the FWHM of 25.3 nm was much narrower than that reported in literatures. The calculated EQE and wall plug efficiency (WPE) of the chip were 46.2% and 41.9%, respectively. Table II showed the wavelength, EQE, WPE, FWHM, and forward voltage at 20 A/cm^2 of different green LEDs reported in recent literatures [11]–[14], [27]. It showed that the EQE of this work was higher, along with the

TABLE II
REPORTED GREEN LED CHIP DATA AT 20 A/cm^2

Year	Ref.	Wavelength (nm)	EQE at 20 A/cm^2 (%)	WPE at 20 A/cm^2 (%)	FW HM (nm)	Voltage (V)
2016	[11]	526.6	30.2	20.3	32.7	3.50
2018	[12]	529.3	29.5	19.7	33.0	3.50
2019	[13]	525.0	41.6	36.0	34.8	2.73
2018	[27]	527.0	38.4	31.6	31.7	2.86
2020	[14]	529.0	41.9	35.6	32.2	2.76
2021	This work	526.4	46.1	41.9	25.3	2.59

much lower forward voltage, which made the WPE significantly improved. Based on the data of literatures and major commercial LEDs, the WPE values at 20 A/cm^2 of these LEDs with different wavelengths were plot in Fig. 6(c). It was shown that the WPE of both literature-reported and commercial green LEDs were lower than 38%, which was much lower than that of commercial red and blue LEDs. The WPE of this work had an obvious leap forward (as shown by the green pentagram in the Fig. 6(c)) and diminished the difference between green LEDs and blue/red LEDs. It demonstrated that the ex-situ sputtered AlNO buffer layer was a feasible method to improve the WPE of InGaN LEDs.

IV. CONCLUSION

The method to improve efficiency of InGaN green LEDs by adjusting AlNO buffer layer lattice constant was reported. By optimizing the O_2 flow rate during AlNO sputtering process, the lattice constant of the AlNO buffer was adjusted and its lattice mismatch with PSS decreased. As a result, the dislocation density and the in-plane compressive stress were greatly reduced, while the interface quality of the InGaN/GaN multiple quantum wells and the uniformity of the indium composition were improved. The QCSE was alleviated which was proved by the enhanced INT and the shorter wavelength in photoluminescence. As a result, the high EQE of 46.2% and WPE of 41.9% were obtained at a typical working current density of 20 A/cm^2. This technique paves the way for stress manipulation in nitride LEDs grown on sapphire substrates covering from ultraviolet to infrared.

REFERENCES

[1] Y. Narukawa, M. Ichikawa, D. Sanga, M. Sano, and T. Mukai, "White light emitting diodes with super-high luminous efficacy," *J. Phys. D: Appl. Phys.*, vol. 43, no. 35, Aug. 2010, Art. no. 354002, doi: 10.1088/0022-3727/43/35/354002.

[2] M. H. Crawford, "LEDs for solid-state lighting: Performance challenges and recent advances," *IEEE J. Sel. Topics Quantum Electron.*, vol. 15, no. 4, pp. 1028–1040, Jul./Aug. 2009.

[3] M. R. Krames *et al.*, "Status and future of high-power light-emitting diodes for solid-state lighting," *J. Display Technol.*, vol. 3, no. 2, pp. 160–175, Jun. 2007.

[4] M. R. Krames *et al.*, "High-power truncated-inverted-pyramid $(Al_xGa_{1-x})_{0.5}In_{0.5}P$/GaP light-emitting diodes exhibiting >50% external quantum efficiency," *Appl. Phys. Lett.*, vol. 75, no. 16, pp. 2365–2367, Oct. 1999.

[5] T. Mukai, H. Narimatsu, and S. Nakamura, "Amber Ingan-based light-emitting diodes operable at high ambient temperatures," *Japan. J. Appl. Phys.*, vol. 37, no. 5A, pp. L479–L481, May 1998.

[6] S. F. Chichibu, Y. Kawakami, and T. Sota, "Emission mechanisms and excitons in GaN and InGaN bulk and QWs," in *Introduction to Nitride Semiconductor Blue Lasers and Light Emitting Diodes*. 1st ed., S. Nakamura, Ed. London, U.K.: CRC Press, 2000, pp. 153–271.

[7] X. A. Cao, "III–Nitride light-emitting diodes on novel substrates," in *Wide Bandgap Light Emitting Materials and Devices*, 1st ed., N. F. Gertrude, Ed. New Jersey, NJ, USA: Wiley-VCH, 2007, pp. 1–48.

[8] J. H. Ryou, P. D. Yoder, J. Liu, Z. Lochner, and R. D. Dupuis, "Control of quantum-confined stark effect in Ingan-based quantum wells," *IEEE J. Sel. Topics Quantum Electron.*, vol. 15, no. 4, pp. 1080–1091, Jul./Aug. 2009.

[9] C. Wetzel *et al.*, "Development of high-power green light emitting diode chips," *Mater. Res. Soc. Internet J. Nitride Semicond. Res.*, vol. 10, Sep. 2005, Art. no. e2.

[10] G. Li *et al.*, "GaN-based light-emitting diodes on various substrates: A critical review," *Rep. Prog. Phys.*, vol. 79, no. 5, Apr. 2016, Art. no. 056501.

[11] A. I. Alhassan *et al.*, "High luminous efficacy green light-emitting diodes with AlGaN cap layer," *Opt. Exp.*, vol. 24, no. 16, pp. 17868–17873, Aug. 2016.

[12] A. I. Alhassan *et al.*, "Development of high-performance green c-plane III-nitride light-emitting diodes," *Opt. Exp.*, vol. 26, no. 5, pp. 5591–5601, Mar. 2018.

[13] Q. Lv *et al.*, "Realization of highly efficient InGaN green LEDs with sandwich-like multiple quantum well structure: Role of enhanced interwell carrier transport," *ACS Photon.*, vol. 6, no. 1, pp. 130–138, Jul. 2018.

[14] Q. Lv *et al.*, "Analysis of dominant non-radiative recombination mechanisms in InGaN green LEDs grown on silicon substrates," *J. Lumin.*, vol. 222, Jun. 2020, Art. no. 117186.

[15] J. H. Ryou *et al.*, "Control of quantum-confined Stark effect in InGaN/GaN multiple quantum well active region by p-type layer for III-nitride-based visible light emitting diodes," *Appl. Phys. Lett.*, vol. 92, no. 10, Aug. 2008, Art. no. 101113.

[16] S. P. Chang *et al.*, "Characteristics of efficiency droop in GaN-based light emitting diodes with an insertion layer between the multiple quantum wells and n-GaN layer," *Appl. Phys. Lett.*, vol. 97, no. 25, Dec. 2010, Art. no. 25114.

[17] X. A. Cao, "Green nitride LEDs," in *GaN and ZnO-Based Materials and Devices*. S. Pearton, Ed., 1st ed. Berlin, Germany: Springer, 2012, pp. 121–152.

[18] J. A. Kohn, P. G. Cotter, and R. A. Potter, "Synthesis of aluminum nitride monocrystals," *Amer. Mineralogist*, vol. 41, no. 3-4, pp. 355–359, Apr. 1956.

[19] J. Graham, "Lattice spacings and colour in the system alumina-chromic oxide," *J. Phys. Chem. Solids*, vol. 17, no. 1-2, pp. 18–25, Dec. 1960.

[20] Y. Repelin and E. Husson, "Etudes structurales d'alumines de transition. I-alumines gamma et delta," *Mater. Res. Bull.*, vol. 25, no. 5, pp. 611–621, May 1990.

[21] S. R. Lee *et al.*, "Effect of threading dislocations on the Bragg peak-widths of GaN, AlGaN, and AlN heterolayers," *Appl. Phys. Lett.*, vol. 86, no. 24, Jun. 2005, Art. no. 241904.

[22] V. M. Kaganer, O. Brandt, A. Trampert, and K. H. Ploog, "X-ray diffraction peak profiles from threading dislocations in GaN epitaxial films," *Phys. Rev. B*, vol. 72, no. 4, Jul. 2005, Art. no. 045423.

[23] M.A.G. Halliwell, M.H. Lyons, and M.J. Hill, "The interpretation of X-ray rocking curves from III–V semiconductor device structures," *J. Cryst. Growth*, vol. 68, no. 3, pp. 523–531, Sep. 1984.

[24] A. Y. Nikulin, O. Sakata, H. Hashizume, and P. V. Petrashen, "Mapping of two-dimensional lattice distortions in silicon crystals at submicrometer resolution from X-ray rocking-curve data," *J. Appl. Crystallogr.*, vol. 27, no. 3, pp. 338–344, Jun. 1994.

[25] D. G. Zhao *et al.*, "An experimental study about the influence of well thickness on the electroluminescence of InGaN/GaN multiple quantum wells," *J. Alloys Compounds*, vol. 489, no. 2, pp. 461–464, Jan. 2010.

[26] D. G. Zhao *et al.*, "Effect of in incorporation parameters on the electroluminescence of blue–violet InGaN/GaN multiple quantum wells grown by metalorganic chemical vapor deposition," *J. Alloys Compounds*, vol. 540, no. 5, pp. 46–48, Nov. 2012.

[27] P. P. Li, Y. B. Zhao, H. J. Li, J. M. Che, and G. H. Wang, "Very high external quantum efficiency and wall-plug efficiency 527 nm InGaN green LEDs by MOCVD," *Opt. Exp.*, vol. 26, no. 25, pp. 33108–33115, Dec. 2018.